Published in final edited form as:

Clin Cancer Res. 2009 October 01; 15(19): 6148–6157. doi:10.1158/1078-0432.CCR-09-1039.

Vorinostat Inhibits Brain Metastatic Colonization in a Model of Triple-Negative Breast Cancer and Induces DNA Double-Strand Breaks

Diane Palmieri[1], **Paul R. Lockman**[5], **Fancy C. Thomas**[5], **Emily Hua**[1], **Jeanne Herring**[6], **Elizabeth Hargrave**[1], **Matthew Johnson**[1], **Natasha Flores**[1], **Yongzhen Qian**[6], **Eleazar Vega-Valle**[6], **Kunal S. Taskar**[5], **Vinay Rudraraju**[5], **Rajendar K. Mittapalli**[5], **Julie A. Gaasch**[5], **Kaci A. Bohn**[5], **Helen R. Thorsheim**[5], **David J. Liewehr**[2], **Sean Davis**[3], **John F. Reilly**[7], **Robert Walker**[3], **Julie L. Bronder**[1], **Lionel Feigenbaum**[6], **Seth M. Steinberg**[2], **Kevin Camphausen**[4], **Paul S. Meltzer**[3], **Victoria M. Richon**[7], **Quentin R. Smith**[5], **Patricia S. Steeg**[1]

[1]Women's Cancers Section, Laboratory of Molecular Pharmacology [2]Biostatistics and Data Management Section [3]Molecular Genetics Section, Genetics Branch [4]Imaging and Molecular Therapeutics Section, Radiation Oncology Branch, National Cancer Institute/NIH, Bethesda, Maryland [5]Department of Pharmaceutical Sciences, School of Pharmacy, Texas Tech University Health Sciences Center, Amarillo, Texas [6]Laboratory Animal Sciences Program, Science Applications International Corporation-Frederick, National Cancer Institute/NIH, Frederick, Maryland [7]Cancer Biology and Therapeutics, Merck Research Laboratories, Boston, Massachusetts

Abstract

Purpose: As chemotherapy and molecular therapy improve the systemic survival of breast cancer patients, the incidence of brain metastases increases. Few therapeutic strategies exist for the treatment of brain metastases because the blood-brain barrier severely limits drug access. We report the pharmacokinetic, efficacy, and mechanism of action studies for the histone deactylase inhibitor vorinostat (suberoylanilide hydroxamic acid) in a preclinical model of brain metastasis of triple-negative breast cancer.

Experimental Design: The 231-BR brain trophic subline of the MDA-MB-231 human breast cancer cell line was injected into immunocompromised mice for pharmacokinetic and metastasis studies. Pharmacodynamic studies compared histone acetylation, apoptosis, proliferation, and DNA damage *in vitro* and *in vivo*.

Results: Following systemic administration, uptake of [^{14}C]vorinostat was significant into normal rodent brain and accumulation was up to 3-fold higher in a proportion of metastases

Requests for reprints: Diane Palmieri, 37 Convent Drive, Building 37, Room 1122, MSC 4254, Bethesda, MD 20892. Phone: 301-402-2732; Fax: 301-402-8910, palmierd@mail.nih.gov.
Current address for J.L. Bronder: Office of Science Planning and Assessment, National Cancer Institute/NIH, Rockville, Maryland.

Disclosure of Potential Conflicts of Interest
J. F. Reilly and V. M. Richon, employment, Merck.

Note: Supplementary data for this article are available at Clinical Cancer Research Online (http://clincancerres.aacrjournals.org/).

formed by 231-BR cells. Vorinostat prevented the development of 231-BR micrometastases by 28% ($P = 0.017$) and large metastases by 62% ($P < 0.0001$) compared with vehicle-treated mice when treatment was initiated on day 3 post-injection. The inhibitory activity of vorinostat as a single agent was linked to a novel function *in vivo*: induction of DNA double-strand breaks associated with the down-regulation of the DNA repair gene Rad52.

Conclusions: We report the first preclinical data for the prevention of brain metastasis of triple-negative breast cancer. Vorinostat is brain permeable and can prevent the formation of brain metastases by 62%. Its mechanism of action involves the induction of DNA double-strand breaks, suggesting rational combinations with DNA active drugs or radiation.

Significant advances have been made in the treatment of primary breast cancer; one of the unfortunate complications of this progress is an increase in the incidence of brain metastases (reviewed in refs. 1, 2). Combinations of cytotoxic and targeted therapies have afforded metastatic breast cancer patients' clinical responses or stable disease, but the poor penetration of these drugs into the brain and leptomeninges creates a "sanctuary site" for recurrence. With an increased number of metastatic breast cancer patients having stable disease or responding to treatment systemically when they develop brain metastases, there is a need to find agents to treat the central nervous system lesions present in otherwise healthy and functional patients given that the 1-year survival estimate after diagnosis of a brain metastasis is only ~20% (2).

The blood-brain barrier (BBB) is the prime determinant of the brain's status as a chemotherapy sanctuary site for tumor cells. The BBB consists of capillary endothelial cells that lack fenestrations, have low pinocytotic activity and high electrical resistance, and are connected by continuous tight junctions to keep undesirable agents from entering the brain. The basement membrane, pericytes, extracellular matrix, and feet of astrocytes that line the abluminal side of the endothelial cells further restrict movement of molecules out of the circulation (reviewed in refs. 3–5). Most molecules that cross the BBB are small in molecular weight, nonpolar, and hydrophobic, permitting diffusion through lipid bilayer membranes (6). Some molecules that are required for cerebral metabolism, such as amino acids, glucose, and nucleosides, are shuttled into the brain by specific facilitated transport systems at the BBB. However, many substances, including most chemotherapeutics, are actively transported out of brain at the BBB by efflux carriers such as P-glycoprotein, thereby limiting central nervous system exposure (5). Common wisdom dictates that the breach in the BBB created by the invasion and colonization of a tumor cell to form a metastasis, and the progressively growing metastasis, opens the permeability of the BBB to create a blood-tumor barrier, although very little quantified data exist on this topic (7). We used a quantitative experimental brain metastasis assay of triple-negative breast cancer (8) to evaluate drugs that may be BBB-permeable, but not in the traditional armamentarium of breast cancer agents, to identify new therapies for the treatment of breast cancer brain metastasis. Herein, we report data for the histone deacetylase inhibitor, vorinostat (suberoylanilide hydroxamic acid), currently Food and Drug Administration approved for the treatment of refractory cutaneous T-cell lymphoma.

In vitro, histone deacetylase inhibitors regulate the acetylation status of histones with subsequent effects on chromatin structure and gene transcription (9, 10). Vorinostat and other histone deacetylase inhibitors also affect the acetylation of nonhistone proteins, block proliferation, generate oxidative species, induce apoptosis, and enhance radiation cytotoxicity (reviewed in refs. 10, 11). Preclinical mouse data showed an inhibition of primary tumor growth in multiple model systems (12–15). There are limited data investigating vorinostat in the metastatic setting. Surprisingly, little data have been published to confirm that the *in vitro* actions of vorinostat are operative *in vivo*. Herein, we report the pharmacology, efficacy, and *in vivo* mechanism of action of vorinostat for the prevention of brain metastases from triple-negative breast cancer.

Materials and Methods

Materials.

Vorinostat was provided by Cancer Therapy Evaluation Program, National Cancer Institute.

In situ *brain perfusion*.

The right common carotid artery of pentobarbital-anesthetized adult Sprague-Dawley rats was catheterized and the right external carotid artery was ligated with surgical silk. The right common carotid artery catheter was connected to a syringe containing [^{3}H]vorinostat (0.2 μCi/mL; 8 nmol/L) and [^{14}C]sucrose (0.1 μCi/mL), as a vascular marker, dissolved in bicarbonate-buffered physiologic saline (16). Perfusion was initiated by severing the right cardiac atrium and infusing tracer-containing perfusion fluid into the right common carotid artery with a pump (5 mL/min). After 30 to 120 s, the perfusion pump was stopped, and weighed samples of brain and perfusion fluid were collected for analysis of ^{3}H content by liquid scintillation counting. Brain [^{3}H]vorinostat uptake was expressed as a distribution space (mL/g) calculated as the measured brain ^{3}H content (dpm/g), corrected for intravascular tracer using [^{14}C]sucrose, divided by the perfusion fluid [^{3}H]vorinostat concentration (dpm/mL; ref. 17). The BBB permeability-surface area product to free drug (PS; mL/s/g) for unidirectional uptake was obtained as the slope of the linear regression of vascularly corrected brain ^{3}H uptake space (mL/g) versus perfusion time (s; ref. 16). In some experiments, vascular [^{3}H]vorinostat was removed from the brain with a short (30 s) post-perfusion wash with tracer-free fluid. The [^{3}H]suberoylanilide hydroxamic acid octanol/water distribution coefficient was measured at pH 7.4 with physiologic saline buffer using the shake flask method as described (16).

Animal experiments.

All experiments were conducted under an approved animal use agreement with the National Cancer Institute. For efficacy studies, 5- to 7-week-old female BALB/c nude mice (Charles River Laboratories) were inoculated with 175,000 231-BR cells in 0.1 mL PBS in the left ventricle. Three days after tumor cell inoculation, mice were randomized to treatment groups. One group began vorinostat treatment (150 mg/kg) on day 3 post-injection and a second group began vehicle treatment. Four days later, a third group began vorinostat treatment 7 days post-injection and the final group began treatment 14 days post-injection.

Vorinostat was administered via intraperitoneal injection once daily, 7 days a week. The drug vehicle solution was 10% DMSO and 45% polyethylene glycol 400.

Mice were euthanized under CO_2 anesthesia 24 to 26 days post-injection and brains were excised. Mouse brains were bisected along the sagittal plane and the right hemisphere of the brain was fixed in 4% paraformaldehyde for 24 h at 4°C, transferred to 20% sucrose overnight at 4°C, and frozen in OCT. The left hemisphere was formalin-fixed and paraffin-embedded for immunohistochemistry. Ten serial sections (10 μm thick) every 300 μm through the right hemisphere were analyzed at a ×50 magnification on a Zeiss microscope, containing an ocular grid with squares of 0.8 mm^2. Every micrometastasis or large metastasis (>300 μm along the longest axis) in each section was tabulated.

For brain [^{14}C]vorinostat quantitative autoradiography, mice bearing 231-BR brain metastases were anesthetized with sodium pentobarbital and administered 150 mg/kg [^{14}C]vorinostat (2.5–5.0 μCi/mouse) and 3 kDa Texas Red dextran (1.5 mg/mouse) into the femoral vein at 30 and 10 m, respectively, before death. The brain was removed from the skull and promptly frozen in isopentane (−70°C). The brain was cut into 20 μm coronal sections and tissue sections were analyzed for green and red fluorescence using an Olympus MVX10 microscope. Tissue radioactivity was quantified using a Fujifilm FLA7000 phosphoimager with the MCID analysis program and ^{14}C autoradiography standards (Amersham Biosciences).

Western blot analysis.

Cells were treated with vorinostat at the concentrations indicated for the times given before lysis. Cells were lysed in radioimmunoprecipitation assay buffer containing complete mini EDTA-free protease inhibitor cocktail (Roche). Total lysates (50 μg/lane) were resolved by SDS-PAGE and transferred to nitrocellulose membranes. Immunoblot analysis was done per standard procedures. Primary antibodies against the following proteins used were acetyl histone H3 (Millipore), acetyl histone H4 (Millipore), α-tubulin (Oncogene), and Hairy and enhancer of split homologue-1 (Hes1; Novus Biologicals). Horseradish peroxidase–conjugated secondary antibodies were used at dilutions of 1:5,000. Proteins were visualized using enhanced chemiluminescence and autoradiography.

Cell death ELISA assay.

Apoptosis was measured using the Cell Death ELISA^{Plus} (Roche) according to the manufacturer’s instructions.

Clonogenic assay.

Cells were plated as a single-cell density and treated with vehicle or vorinostat 24 h later and every 4 days for 12 days. Colonies were fixed with 50% methanol/10% acetic acid and stained with crystal violet for quantification.

Cell migration assay.

Boyden chamber motility assays were conducted as described previously (8).

Neutral comet assay.

A kit from Trevigen was used according to the recommendations from the manufacturer. DNA was stained with propidium iodide and digital fluorescent images were captured on a Zeiss Axioskop 2 microscope using OpenLab software (Improvision). At least 25 images per time point were evaluated with olive tail moment determined using CASP software (18).

Immunohistochemistry.

Formalin-fixed, paraffin-embedded tissue sections were used for acetylated histone H3 lysine 9 and acetylated histone H4 lysine 8 (Cell Signaling Technology), Ki-67 and proliferating cell nuclear antigen (PCNA; DAKO), and Rad52 (Cell Signaling Technology) staining. Immunodetection was obtained with the EnVision+ horseradish peroxidase system according to the manufacturer's instructions (DAKO).

Immunofluorescence.

Freshly cut, frozen sections were air-dried before staining. Sections were stained with α-γ-histone H2AX (S139; Novus Biologicals). α-Rabbit Alexa Fluor 555 was used for detection. Nuclei were counterstained with 4′,6-diamidino-2-phenylindole. Images were captured on a Zeiss LSM 510 confocal microscope.

Statistical analysis.

A one-, two-, or three-way ANOVA was done on the data. Nonweighted, weighted, and mixed-model ANOVAs were used as appropriate. For the mixed-model ANOVA, experiment was the random effect. Residuals were examined for normality and homogeneity and were partitioned if necessary. All *P* values are two-sided and were adjusted using Dunnett's method if more than one group was compared with a control group. For quantitative reverse transcription-PCR relative expression data, means from vehicle- and vorinostat-treated mice were compared using two-way ANOVA. All *P* values are two-tailed.

Results

Vorinostat permeability in the normal brain and experimental brain metastases.

Using the *in situ* brain perfusion technique, [^{3}H]vorinostat was taken up into normal brain with a BBB PS of $1.4 \pm 0.3 \times 10^{-4}$ mL/s/g (Fig. 1A). The Y axis intercept (0.0102 ± 0.0018 mL/g) of the uptake plot exceeded zero ($P < 0.05$) and was removed with a brief (30 s) post-perfusion wash with tracer-free fluid, consistent with a small component of vorinostat binding to the vascular endothelium. When plotted versus the octanol/water distribution coefficient, a measure of lipophilicity, the BBB PS to vorinostat fell >2 orders of magnitude below that predicted for BBB passive diffusion (Fig. 1B). Co-perfusion with verapamil (150 μmol/L), an inhibitor of active efflux transport, increased the BBB PS to [^{3}H]vorinostat by >2 fold ($P < 0.05$; data not shown), suggestive of a role of active efflux in limiting vorinostat distribution. The log octanol/water distribution coefficient for [^{3}H]vorinostat at pH 7.4 equaled 1.07 ± 0.01.

To evaluate the ability of vorinostat to distribute to brain and brain metastasis *in vivo*, mice with 231-BR-EGFP metastases were administered 150 mg/kg [^{14}C]vorinostat intravenously

30 min before death. Animals also received 1.5 mg 3 kDa Texas Red dextran (a passive permeability marker) 10 min before death to visualize leaky tumor blood vessels. A representative coronal brain section shows EGFP-labeled metastatic clusters, 3 kDa Texas Red dextran distribution, and ^{14}C distribution in a [^{14}C]vorinostat-treated mouse (Fig. 1C). The three lesions showed variability in leakiness to 3 kDa Texas Red dextran. In other metastatic lesions and in micrometastases in the tissue section, ^{14}C concentration did not differ from that of surrounding brain tissue. These same patterns were seen in all animals evaluated ($n = 5$).

The average brain/blood concentration ratio at 30 min equaled 0.075 ± 0.011 mL/g (mean ± SE; $n = 5$), showing significant uptake of [^{14}C]vorinostat into brain above that of residual blood volume (~0.01 mL/g). At 30 min, blood ^{14}C concentration equaled 234 ± 48 nCi/mL, equivalent to a vorinostat concentration of 140 ± 28 μg/mL ($n = 5$). The data indicate that vorinostat is taken up into normal brain to a significant extent, reaching a level ~5 to 7 times greater at 30 min than that expected for residual blood in the brain vasculature.

Enhanced ^{14}C uptake was detectable at 61, 56, and 48 nCi/g in three metastatic lesions in the tissue section, which exceeded normal brain ^{14}C concentration (30 ± 2 nCi/g) by 1.6- to 2-fold. Vorinostat, therefore, distributes heterogeneously among brain metastases, with some metastatic lesions showing no difference in concentration from surrounding brain and others showing ^{14}C elevations of up to 3-fold.

Vorinostat prevention of 231-BR brain metastases.

Given the uptake of vorinostat into the normal brain and enhancement of uptake in a proportion of brain metastases, we hypothesized that vorinostat could inhibit brain metastasis. 231-BR cells were injected into the left ventricle of mice and mice were treated with vehicle or vorinostat intraperitoneally starting 3 days post-injection. At necropsy, 10 sagittal H&E-stained step sections through one hemisphere of the brain were counted using an ocular micrometer to distinguish micrometastases and large metastases, the latter comparable in one-dimensional size to a magnetic resonance imaging–detectable metastasis in a human brain as reported previously (19). Initial experiments established that 150 mg/kg vorinostat showed efficacy with minimal side effects (Supplementary Table S1).

Table 1 presents a combined analysis of two independent experiments examining the ability of vorinostat to prevent or treat 231-BR brain metastases. Four experimental arms are listed, mice receiving either vehicle or vorinostat beginning 3 days post-injection, and mice receiving drug beginning either 7 or 14 days post-injection. By the latter date, micrometastases were evident in sectioned brains (data not shown). Representative images of whole brains ex vivo are shown in Fig. 2. Vorinostat treatment beginning on day 3 significantly reduced the formation of large metastases from a mean of 7.65 per section to 2.89, a 62% reduction ($P < 0.0001$). A significant reduction in micrometastases was observed, from a mean of 170 to 122, a 28% reduction ($P = 0.017$). Delay of vorinostat treatment to 7 days post-injection produced a 35% reduction over vehicle-treated controls ($P = 0.008$). A further delay in vorinostat treatment until day 14 post-injection reduced large metastases by 22% but was not statistically significant. The data indicate that vorinostat significantly reduced the number of micrometastases and large brain metastases in this

triple-negative model of breast cancer but that it was most efficacious when administered early.

Discordant histone acetylation, cell cycle, and apoptotic effects of vorinostat *in vitro* and *in vivo*.

The *in vitro* activities of vorinostat on 231-BR cells are shown on Fig. 3. Increased acetylation of histone H3 and H4 was noted from 0.5 to 10 μmol/L vorinostat (Fig. 3A). Vorinostat altered the cell cycle distribution of 231-BR cells, with an increased percentage of cells in the G_0-G_1 phases (43% versus 62–70% of cells) and a corresponding decrease in S phase (37% versus 10–15%), indicative of a G_1-S blockade. Induction of apoptosis was evident at 5 to 10 μmol/L vorinostat as measured by a DNA fragmentation ELISA (Fig. 3B) and confirmed to occur through the intrinsic pathway (Supplementary Fig. S1). There was no evidence of vorinostat induction of autophagy (Supplementary Fig. S2). Vorinostat also inhibited the clonogenic growth and migration of 231-BR cells (Fig. 3C and D, respectively). Each of these effects of vorinostat was consistent with previously reported studies.

To determine the effect of vorinostat on histone acetylation *in vivo*, mice were necropsied within 4 h of a final dose of vehicle or drug and sections of dissected brains were subjected to immunohistochemistry for acetylated histone H3 (lysine 9) and histone H4 (lysine 8) in a blinded fashion. The percentage and intensity of stained nuclei in both normal brain and metastatic lesions were comparable between the vehicle and 150 mg/kg vorinostat arms (Supplementary Fig. S3). Apoptosis, visualized by either TACS-XL *In situ* Apoptosis Detection kit or cleaved caspase-3 immunofluorescence, was not detectable in sections of 150 mg/kg vorinostat-treated brains (data not shown). Within the sensitivities of the assays used for *in vivo* detection, vorinostat inhibition of brain metastasis was not accompanied by increased histone acetylation or apoptosis in contrast to *in vitro* data.

Immunohistochemistry was conducted on sections of dissected brains from vehicle-treated or 150 mg/kg vorinostat-treated mice to determine its effects on the cell cycle *in vivo*. The percentage of Ki-67–positive tumor cells in large brain metastases from sections of vehicle-treated or vorinostat (150 mg/kg)–treated mice was determined. Vorinostat induced a 10% absolute decrease (a 19% relative decrease) in Ki-67 labeling, from a weighted mean of 52% to 42%, a trend of more cells in G_0 ($P = 0.18$). To further define the possible effects of vorinostat on the cell cycle, a similar experiment was done using PCNA, indicative of either cells in S phase or cells containing DNA damage (20). Large metastases from vehicle-treated mice contained a weighted mean of 54% PCNA-positive tumor cells; large metastases in brains of mice treated with 150 mg/kg vorinostat contained a weighted mean of 73% PCNA-positive cells, a 19% absolute increase (35% relative increase) over controls ($P = 0.15$). The statistically significant effects of vorinostat on proliferation *in vitro* were, at best, statistical trends *in vivo*. Interestingly, the increase in PCNA staining of large metastases in the brains of vorinostat-treated mice could also represent a response to DNA damage as PCNA is a processivity factor for DNA polymerases in both DNA replication and DNA repair.

Vorinostat induces DNA double-strand breaks in vitro *and* in vivo.

To determine if vorinostat induced DNA damage *in vitro*, immunofluorescence for γ-H2AX (21) was done on 231-BR cells treated with vehicle or 5 μmol/L vorinostat as well as after removal of drug. Cells were scored as either negative (0) or having <20 or >20 γ-H2AX foci per cell (Fig. 4A, *top*). Vehicle-treated cells have a low level of endogenous DNA damage; only 3% of the cells had >20 γ-H2AX foci per cell in contrast to 42% after 2 h of vorinostat treatment (Fig. 4A, *bottom*). Interestingly, 24 h after removal of vorinostat, 50% of the cells had >20 foci per cell, suggesting a lack of DNA repair. To confirm these data, comet assays were done, which quantify DNA fragmentation. 231-BR cells were treated with vehicle or 1 or 5 μmol/L vorinostat *in vitro* for 24 h; the olive tail moment of the comet for the vehicle-treated cells averaged 2.6 over three replicate experiments compared with 12.7 for γ-irradiated cells (data not shown). The olive tail moment was increased 1.6-and 3.6-fold in cells treated with 1 or 5 μmol/L vorinostat, respectively (Fig. 4B; $P < 0.0001$). The data identify a new property of vorinostat as a single agent, the induction of DNA double-strand break (DSB).

To determine if vorinostat induction of DSB occurred *in vivo*, sections of brains from vehicle-treated or 150 mg/kg vorinostat-treated mouse brains were stained for γ-H2AX using immunofluorescence. Representative sections are shown in Fig. 4C; γ-H2AX appears pink on blue 4′,6-diamidino-2-phenylindole–stained nuclei. Whereas some control nuclei contained foci of γ-H2AX, tumor cells treated with vorinostat contained visibly greater γ-H2AX, to the point where some nuclei appear homogeneously stained. The percentage of γ-H2AX–positive tumor cells in large metastases from 4 to 5 mice per group is graphed on Fig. 4D (*left*). γ-H2AX–positive cells ranged from 0 to 6% of tumor cells in vehicle-treated brains with a mean of 3.29%; for 150 mg/kg vorinostat-treated mice, the percentage of γ-H2AX–positive cells ranged from 1% to 14% with a mean of 6.71%, a 104% increase over controls ($P = 0.047$). Similar trends were observed in micrometastatic lesions where vorinostat induced a mean of 12.3% γ-H2AX–positive cells compared with 3.47% in controls, a 254% increase ($P = 0.004$; Fig. 4D, *right*). In conclusion, vorinostat induced DSB in 231-BR cells *in vitro* and *in vivo*, suggesting that it may contribute to its inhibition of brain metastatic colonization.

In vivo *gene expression changes induced by vorinostat inhibition of brain metastasis.*

We performed gene expression profiling on metastases from vehicle- or vorinostat-treated mice to determine if alterations in gene expression were observable that were consistent with the phenotypes observed. Brain metastases from five vehicle-treated mice and six 150 mg/kg vorinostat-treated mice were procured by laser capture microdissection. RNA was extracted from the captured tumor cells from each brain and two rounds of linear amplification was done. The amplified RNA from each mouse was processed separately through microarray hybridization and analysis. One hundred sixteen genes were differentially expressed with a false discovery rate of <5% and at least a 2.5-fold difference in expression. Of those, 63 were downregulated (Supplementary Table S2) and 54 were upregulated (Supplementary Table S3) in the metastases from brains of vorinostat-treated mice. Simple hierarchical clustering of the top 75 differentially expressed genes are shown in Fig. 5A.

Hes1 was the most highly differentially expressed gene in the analysis and was present twice in the top 10. It was downregulated 29.3- and 5.8-fold, respectively. This was validated by quantitative reverse transcription-PCR using cDNA synthesized from RNA obtained from laser-captured tumor cells from the brains of vehicle- and vorinostat-treated mice. Quantitative reverse transcription-PCR analysis of vehicle-treated samples showed a 6.8-fold downregulation of Hes1 ($P = 0.0004$; Supplementary Table S4). A decrease in Hes1 protein expression was also note by Western blot in 231-BR cells treated with vorinostat (Fig. 5B).

Rad52 was downregulated 3.5-fold in the microarray analysis in the vorinostat-treated brain metastases. Rad52 participates in the repair of DNA DSB (22), suggesting that vorinostat-mediated changes in gene expression could inhibit repair of DSB induced by the drug. Quantitative reverse transcription-PCR confirmed a 6-fold downregulation of Rad52 by vorinostat ($P = 0.012$; Supplementary Table S4). Immunohistochemical staining for Rad52 in the mouse brains confirmed decreased Rad52 protein in vorinostat-treated mice compared with controls (Fig. 5C).

Discussion

Brain metastases of breast cancer represent an unmet medical need. A new approach is required for this niche site to identify drugs with both brain permeability and efficacy. These drugs will likely be distinct from traditional breast cancer therapeutic agents, and new trial designs may be needed for their clinical validation. We present pharmacokinetic, efficacy, and pharmacodynamic studies indicating that vorinostat, a histone deacetylase inhibitor approved for refractory T-cell lymphoma, may prevent the brain metastatic colonization of triple-negative breast cancer. We also present a comprehensive comparison of potential *in vitro* and *in vivo* mechanisms of vorinostat activity. A distinct activity, the induction of DNA DSB and their poor repair, was the best measure of brain metastasis prevention, an activity previously unreported in the literature for vorinostat as a single agent.

Vorinostat showed significant uptake into normal brain, reaching a brain/blood concentration ratio at 30 min that exceeded the brain residual blood volume (0.0075–0.015 mL/g) by 5- to 7-fold (23, 24). These data extend previous qualitative, immunohistochemistry-based reports of brain permeability of vorinostat in mouse models of Huntington’s disease and glioma (13, 25). The model system permitted quantification of drug uptake into metastases, with a direct comparison to vascular integrity in each lesion, as determined by ^{14}C autoradiography and 3 kDa fluorescent Texas Red dextran, respectively. Several conclusions emerged. First, there was heterogeneity among metastases, as not all metastases were permeable to the intercellular passive diffusion marker Texas Red dextran. This observation contradicts the conventional wisdom that the BBB is compromised in all “large” brain metastases. Second, in several large metastases, [^{14}C]vorinostat uptake exceeded that of surrounding brain tissue by up to 3-fold, whereas in other large metastases and in micrometastases there were no differences in [^{14}C]vorinostat distribution from normal brain. The data provide the first quantitative analyses of vorinostat uptake into the central nervous system in a model of experimental brain metastasis. Although vorinostat exhibits many of the structural features recommended for good BBB penetration (26), the BBB PS was lower than expected (Fig. 1B) possibly as a result of active efflux transport at the BBB.

Vorinostat significantly prevented the development of brain metastases of breast cancer in the 231-BR model system. A 62% reduction in large metastases (comparable in size to a magnetic resonance imaging–detectable lesion in a human brain) was observed when vorinostat was administered 3 days post-injection. Consistent with the permeability of vorinostat into normal brain, a 28% reduction was observed in micrometastases, indicating that the basal concentrations of vorinostat observed in normal brain and micrometastases were sufficient for biological activity. Vorinostat has shown preclinical activity in other cancer model systems, including reductions in tumor size and increases in lifespan; to our knowledge, no studies have been conducted in the metastatic setting. The importance of preclinical drug testing in the metastatic setting has recently been highlighted in the literature where antiangiogenic therapies have been shown to decrease primary tumor size but increase tumor aggressiveness and metastasis (27, 28).

In addition, an understanding of the mechanism of drug action *in vivo* is key to the development of useful pharmacodynamic markers and rational combinations. Although numerous reports have investigated the mechanism of action of vorinostat in vitro, few have confirmed the data *in vivo*. We conducted a pharmacodynamic analysis of several prominent aspects of vorinostat activity: histone acetylation, gene expression changes, proliferation, and apoptosis. *In vitro* prominent apoptosis was induced but was undetectable in the brain *in vivo*. Increased histone acetylation was observed on Western blot *in vitro* but not by immunohistochemistry *in vivo* in this model system. In other model systems, increased histone acetylation has been detected *in vivo* (13); it remains possible that subtle changes occurred here, but the assay lacked sensitivity to detect them.

Despite the lack of observable histone acetylation or apoptosis, vorinostat prevented the development of both micrometastases and large metastases. Two potential mechanisms of action have been identified *in vivo*. First, Ki-67 labeling indicated a trend (30% increase) in tumor cells that have exited the cell cycle. Similar findings were noted *in vitro* where flow cytometry analysis showed an increased number of cells in G_0G_1 after vorinostat treatment. No significant change in p21 or other reported antiproliferative mediators of vorinostat were noted by microarray analysis. Downregulation of Hes1 was observed in vorinostat, compared with vehicle-treated brain metastases, and could contribute to this phenotype.

In contrast to the Ki-67 staining, increased PCNA staining of vorinostat-treated brain metastases *in vivo* was noted and suggested the novel possibility that this drug could induce DNA damage as a mechanism of action. Although vorinostat has been reported to synergize with radiation and DNA-damaging agents (29–31), a role for this drug as a single agent in the formation of DNA DSB is almost completely unstudied. γ-H2AX foci, indicative of DNA DSB, were increased 2-fold in the metastases of vorinostat-treated mice compared with vehicle treatment ($P = 0.029$). In vitro, vorinostat induced formation of nitric oxide by 231-BR cells, which may be responsible for induction of DNA DSB.[8] *In vitro* data suggested that both the induction of DNA DSB by vorinostat and a deficient repair in the γ-H2AX foci persisted after removal of drug. Microarray analysis identified the downregulation of Rad52 as a consequence of vorinostat treatment *in vivo*. Rad52 is best

[8]Dr. David Wink, National Cancer Institute, personal communication.

known as part of the strand exchange machinery in homologous recombination DSB repair (22, 32, 33). Decreased Rad52 may perpetuate the appearance of DNA DSB by impairing their repair. The data indicate a new potential mechanism of action for vorinostat *in vivo* and is consistent with published reports using other histone-modifying agents in the induction of DNA DSB in hematopoietic cells (34).

The simplest scenario for vorinostat inhibition of metastatic colonization posits that the drug induces DNA DSB and downregulates Rad 52, involved in DSB repair. The DNA damage as well as other changes in gene expression (Hes1) result in a slower rate of tumor cell outgrowth.

Brain metastases of breast cancer represent an increasing problem, primarily concentrated in the triple-negative and HER-2–positive subsets of patients. Vorinostat stands as a novel type of drug, not included in the standard of care for breast cancer but exhibiting brain permeability and the ability to prevent the formation of brain metastases in a preclinical model. Vorinostat has not shown significant single-agent activity against widely metastatic breast cancer, although it exhibited a favorable toxicity profile and 4 of 14 patients exhibited stable disease with time to progression ranging from 4 to 14 months (35). However, the preclinical and clinical activity of drugs to prevent metastases may be greater than that to eliminate an already established large lesion (36, 37). Trials for the prevention of brain metastases could enroll patients in the metastatic setting but would require relatively long follow-up (36); alternatively, patients with brain metastases are at risk for the development of additional brain metastases, and a preventive effect could be tested in this setting. We present the first data indicating that vorinostat induced DNA DSB *in vivo*. These data add to the list of *in vivo* pharmacodynamic markers of activity and may justify rational combinations with DNA-damaging drugs and/or radiation in further therapeutic efforts (38).

Supplementary Material

Refer to Web version on PubMed Central for supplementary material.

Acknowledgments

Grant support: Intramural Program of the National Cancer Institute and Department of Defense Breast Cancer Research Program grant W81XWH-062-0033.

References

1. Lin N, Bellon J, Winer E. CNS metastases in breast cancer. J Clin Oncol 2004;22:3608–17. [PubMed: 15337811]
2. Weil R, Palmieri D, Bronder J, Stark A, Steeg P. Breast cancer metastasis to the central nervous system. Am J Pathol 2005;167:913–20. [PubMed: 16192626]
3. Bart J, Groen H, Hendrikse N, van der Graaf W, Vaalburg W, deVries E. The blood-brain barrier and oncology: new insights into function and modulation. Cancer Treat Rev 2000;26:449–62. [PubMed: 11139374]
4. Kniesel U, Wolburg H. Tight junctions of the blood-brain barrier. Cell Mol Neurobiol 1997;20: 57–76.
5. Deeken JF, Loscher W. The blood-brain barrier and cancer: transporters, treatment, and Trojan horses. Clin Cancer Res 2007;13:1663–74. [PubMed: 17363519]

6. Mahar Doan KM, Humphreys JE, Webster LO, et al. Passive permeability and P-glycoprotein-mediated efflux differentiate central nervous system (CNS) and non-CNS marketed drugs. J Pharmacol Exp Ther 2002;303: 1029–37. [PubMed: 12438524]
7. Fidler I, Yano S, Zhang R, Fujimaki T, Bucana C. The seed and soil hypothesis: vascularisation and brain metastases. Lancet Oncol 2002; 3:53–7. [PubMed: 11905606]
8. Palmieri D, Bronder JL, Herring JM, et al. Her-2 overexpression increases the metastatic outgrowth of breast cancer cells in the brain. Cancer Res 2007;67:4190–8. [PubMed: 17483330]
9. Richon VM, Sandhoff TW, Rifkind RA, Marks PA. Histone deacetylase inhibitor selectively induces $p21^{WAF1}$ expression and gene-associated histone acetylation. Proc Natl Acad Sci U S A 2000;97:10014–9. [PubMed: 10954755]
10. Xu WS, Parmigiani RB, Marks PA. Histone deacetylase inhibitors: molecular mechanisms of action. Oncogene 2007;26:5541–52. [PubMed: 17694093]
11. Richon V. Cancer biology: mechanism of antitumour action of vorinostat (suberoylanilide hydroxamic acid), a novel histone deacetylase inhibitor. Br J Cancer 2006;95: S2–6.
12. Eyupoglu IY, Hahnen E, Buslei R, et al. Suberoylanilide hydroxamic acid (SAHA) has potent anti-glioma properties in vitro, ex vivo and in vivo. J Neurochem 2005;93:992–9. [PubMed: 15857402]
13. Yin D, Ong JM, Hu J, et al. Suberoylanilide hydroxamic acid, a histone deacetylase inhibitor: effects on gene expression and growth of glioma cells in vitro and in vivo. Clin Cancer Res 2007; 13:1045–52. [PubMed: 17289901]
14. Cooper AL, Greenberg VL, Lancaster PS, van Nagell JR Jr., Zimmer SG, Modesitt SC. In vitro and in vivo histone deacetylase inhibitor therapy with suberoylanilide hydroxamic acid (SAHA) and paclitaxel in ovarian cancer. Gynecol Oncol 2007;104:596–601. [PubMed: 17049973]
15. Ugur HC, Ramakrishna N, Bello L, et al. Continuous intracranial administration of suberoylanilide hydroxamic acid (SAHA) inhibits tumor growth in an orthotopic glioma model. J Neurooncol 2007;83:267–75. [PubMed: 17310267]
16. Mandula H, Parepally JM, Feng R, Smith QR. Role of site-specific binding to plasma albumin in drug availability to brain. J Pharmacol Exp Ther 2006;317:667–75. [PubMed: 16410405]
17. Parepally JM, Mandula H, Smith QR. Brain uptake of nonsteroidal anti-inflammatory drugs: ibuprofen, flurbiprofen, and indomethacin. Pharm Res 2006;23:873–81. [PubMed: 16715377]
18. Konca K, Lankoff A, Banasik A, et al. A cross-platform public domain PC image-analysis program for the comet assay. Mutat Res 2003;534: 15–20. [PubMed: 12504751]
19. Gril B, Palmieri D, Bronder JL, et al. Effect of lapatinib on the outgrowth of metastatic breast cancer cells to the brain. J Natl Cancer Inst 2008;100:1092–103. [PubMed: 18664652]
20. Szuts D, Christov C, Kitching L, Krude T. Distinct populations of human PCNA are required for initiation of chromosomal DNA replication and concurrent DNA repair. Exp Cell Res 2005; 311:240–50. [PubMed: 16226749]
21. Sedelnikova OA, Pilch DR, Redon C, Bonner WM. Histone H2AX in DNA damage and repair. Cancer Biol Ther 2003;2:233–5. [PubMed: 12878854]
22. Sung P. Function of yeast Rad52 protein as a mediator between replication protein A and the Rad51 recombinase. J Biol Chem 1997;272: 28194–7. [PubMed: 9353267]
23. Bereczki D, Wei L, Acuff V, et al. Technique-dependent variations in cerebral microvessel blood volumes and hematocrits in the rat. J Appl Physiol 1992;73:918–24. [PubMed: 1400056]
24. Cisternino S, Rousselle C, Dagenais C, Scherrmann JM. Screening of multidrug-resistance sensitive drugs by in situ brain perfusion in P-glycoprotein-deficient mice. Pharm Res 2001; 18:183–90. [PubMed: 11405289]
25. Hockly E, Richon V, Woodman B, et al. Suberoylanilide hydroxamic acid, a histone deacetylase inhibitor, ameliorates motor deficits in a mouse model of Huntington's disease. Proc Natl Acad Sci U S A 2003;100: 2041–6. [PubMed: 12576549]
26. Pajouhesh H, Lenz GR. Medicinal chemical properties of successful central nervous system drugs. NeuroRx 2005;2:541–53. [PubMed: 16489364]
27. Paez-Ribes M, Allen E, Hudock J, et al. Anti-angiogenic therapy elicits malignant progression of tumors to increased local invasion and distant metastasis. Cancer Cell 2009;15: 220–31. [PubMed: 19249680]

28. Ebos JM, Lee CR, Cruz-Munoz W, Bjarnason GA, Christensen JG, Kerbel RS. Accelerated metastasis after short-term treatment with a potent inhibitor of tumor angiogenesis. Cancer Cell 2009;15:232–9. [PubMed: 19249681]

29. Marchion D, Bicaku E, Daud A, Richon V, Sullivan D, Munster P. Sequence-specific potentiation of topoisomerase II inhibitors by the histone deacetylase inhibitor suberoylanilide hydroxamic acid. 2004;92:223–37.

30. Munshi A, Tanaka T, Hobbs ML, Tucker SL, Richon VM, Meyn RE. Vorinostat, a histone deacetylase inhibitor, enhances the response of human tumor cells to ionizing radiation through prolongation of γ-H2AX foci. Mol Cancer Ther 2006;5:1967–74. [PubMed: 16928817]

31. Chinnaiyan P, Vallabhaneni G, Armstrong E, Huang SM, Harari PM. Modulation of radiation response by histone deacetylase inhibition. Int J Radiat Oncol Biol Phys 2005; 62:223–9. [PubMed: 15850925]

32. New JH, Sugiyama T, Zaitseva E, Kowalczykowski SC. Rad52 protein stimulates DNA strand exchange by Rad51 and replication protein A. Nature 1998;391:407–10. [PubMed: 9450760]

33. Song B, Sung P. Functional interactions among yeast Rad51 recombinase, Rad52 mediator, and replication protein A in DNA strand exchange. J Biol Chem 2000;275: 15895–904. [PubMed: 10748203]

34. Gaymes TJ, Padua RA, Pla M, et al. Histone deacetylase inhibitors (HDI) cause DNA damage in leukemia cells: a mechanism for leukemia-specific HDI-dependent apoptosis. Mol Cancer Res 2006;4:563–73. [PubMed: 16877702]

35. Luu TH, Morgan RJ, Leong L, et al. A phase II trial of vorinostat (suberoylanilide hydroxamic acid) in metastatic breast cancer: a California Cancer Consortium study. Clin Cancer Res 2008;14:7138–42. [PubMed: 18981013]

36. Cameron D, Casey M, Press M, et al. A phase III randomized comparison of lapatinib plus capecitabine versus capecitabine alone in women with advanced breast cancer that has progressed on trastuzumab: updated efficacy and biomarker analyses. Breast Cancer Res Treat 2008;112: 533–43. [PubMed: 18188694]

37. Khalili P, Arakelian A, Chen G, Singh G, Rabbani SA. Effect of Herceptin on the development and progression of skeletal metastases in a xenograft model of human breast cancer. Oncogene 2005;24:6657–66. [PubMed: 16091754]

38. Baschnagel A, Russo A, Burgan WE, et al. Vorinostat enhances the radiosensitivity of a breast cancer brain metastatic cell line grown in vitro and as intracranial xenografts. Mol Cancer Ther 2009;8:1589–95. [PubMed: 19509253]

Translational Relevance

Brain metastases of breast cancer are largely untreatable by chemotherapy, as the blood-brain barrier severely limits drug uptake. Here, we show the preclinical pharmacokinetic and efficacy data indicating that vorinostat is brain-permeable, exhibits a several-fold elevation in uptake in a proportion of brain metastases, and can prevent the formation of brain metastases of breast cancers. A new mechanism of action of vorinostat was observed in vitro and *in vivo*, the induction of DNA double-strand breaks that can inform the development of rational combinations.

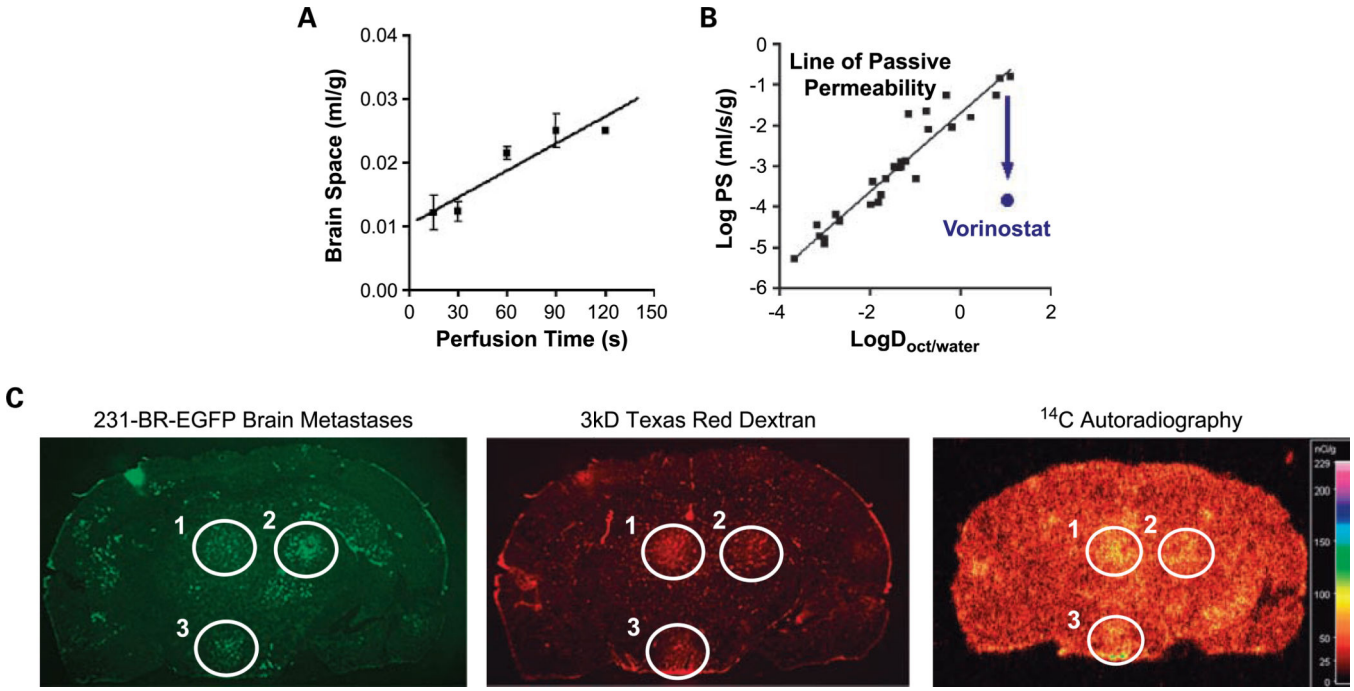

Fig. 1.

Pharmacokinetics of vorinostat uptake in normal brain and in experimental brain metastases of breast cancer. *A*, time course of [^{3}H]vorinostat uptake into normal brain as measured using the *in situ* brain perfusion technique. Mean ± SE for $n = 3$ perfusions. The line is the best-fit linear regression to the data. Brain space (mL/g) was calculated as the vascularly corrected brain ^{3}H concentration divided by the [^{3}H]vorinostat concentration of perfusion fluid. *B*, log BBB PS versus log octanol/water distribution coefficient (logD), a measure of hydrophobicity. The line and black squares are for solutes that cross the BBB by passive diffusion (16). The PS of vorinostat is ~2 logs below that of normal diffusion. *C*, a coronal tissue section from a mouse injected intravenously with 150 mg/kg [^{14}C]vorinostat 30 min before death and 1.5 mg 3 kDa Texas Red dextran 10 min before death. Mice received EGFP-transfected 231-BR cells via intracardiac injection 4 wk before the experiment. Green fluorescent metastatic lesions that formed are circled (*left*). Uptake of the nonspecific 3 kDa Texas Red dextran (red fluorescence; *middle*) and [^{14}C]vorinostat (autoradiogram; *right*) for those circled lesions in the same coronal section is shown. Representative images shown for $n = 5$ mice analyzed.

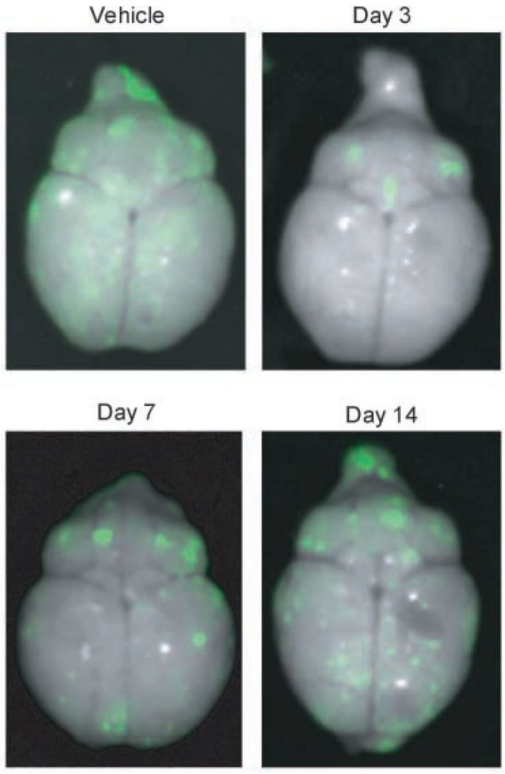

Fig. 2.

Representative dorsal whole-brain images from mice treated with vorinostat. 231-BR-EGFP cells were injected into the left cardiac ventricle of Balb\c mice and vehicle or vorinostat treatment started at days indicated. Brains were dissected at necropsy and imaged using a Maestro 420 Special Imaging System to detect the presence of EGFP-expressing metastases.

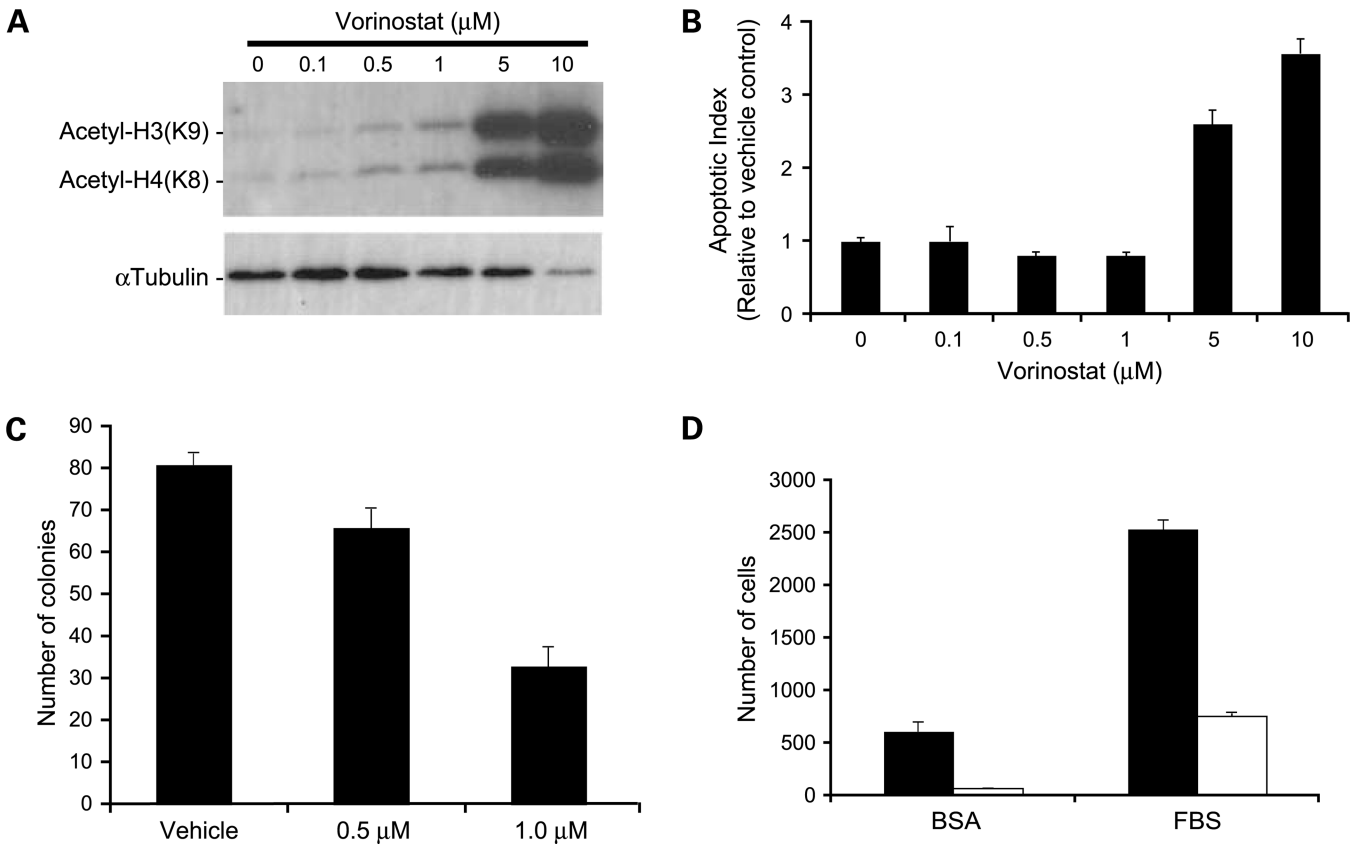

Fig. 3.

In vitro effects of vorinostat on histone acetylation and apoptosis. *A*, Western blot analysis of acetylated histone proteins in 231-BR cells treated with increasing concentrations of vorinostat for 24 h. *B*, apoptosis as measured by the Cell Death Detection ELISA^{PLUS} (Roche). Apoptotic index determined with respect to vehicle control-treated cells given an index of 1 to account for the amount of cell death occurring naturally in a cell population. $P < 0.0001$, ANOVA, post-hoc Dunnett's multiple comparison; $P = 0.014$ for vehicle versus 0.5 μmol/L vorinostat; $P = 0.013$ for vehicle versus 1 μmol/L vorinostat; $P = 0.0001$ for vehicle versus 5 μmol/L vorinostat; $P < 0.0001$ for vehicle versus 10 μmol/L vorinostat. *C*, clonogenic growth in response to 0.5 μmol/L ($P = 0.024$) and 1.0 μmol/L ($P < 0.0001$) vorinostat compared with vehicle control. *P* values were determined by two-way ANOVA with post-hoc Dunnett's multiple comparison. *D*, vorinostat inhibition of cell migration as assessed by Boyden chamber motility experiments. Vorinostat inhibited both unstimulated (bovine serum albumin; $P = 0.0007$) and fetal bovine serum–stimulated ($P < 0.0001$) cell migration. *P* values were determined by three-way ANOVA. *Black columns*, vehicle control; *white columns*, 5 μmol/L vorinostat. Representative experiments of at least three conducted (*A*-*D*).

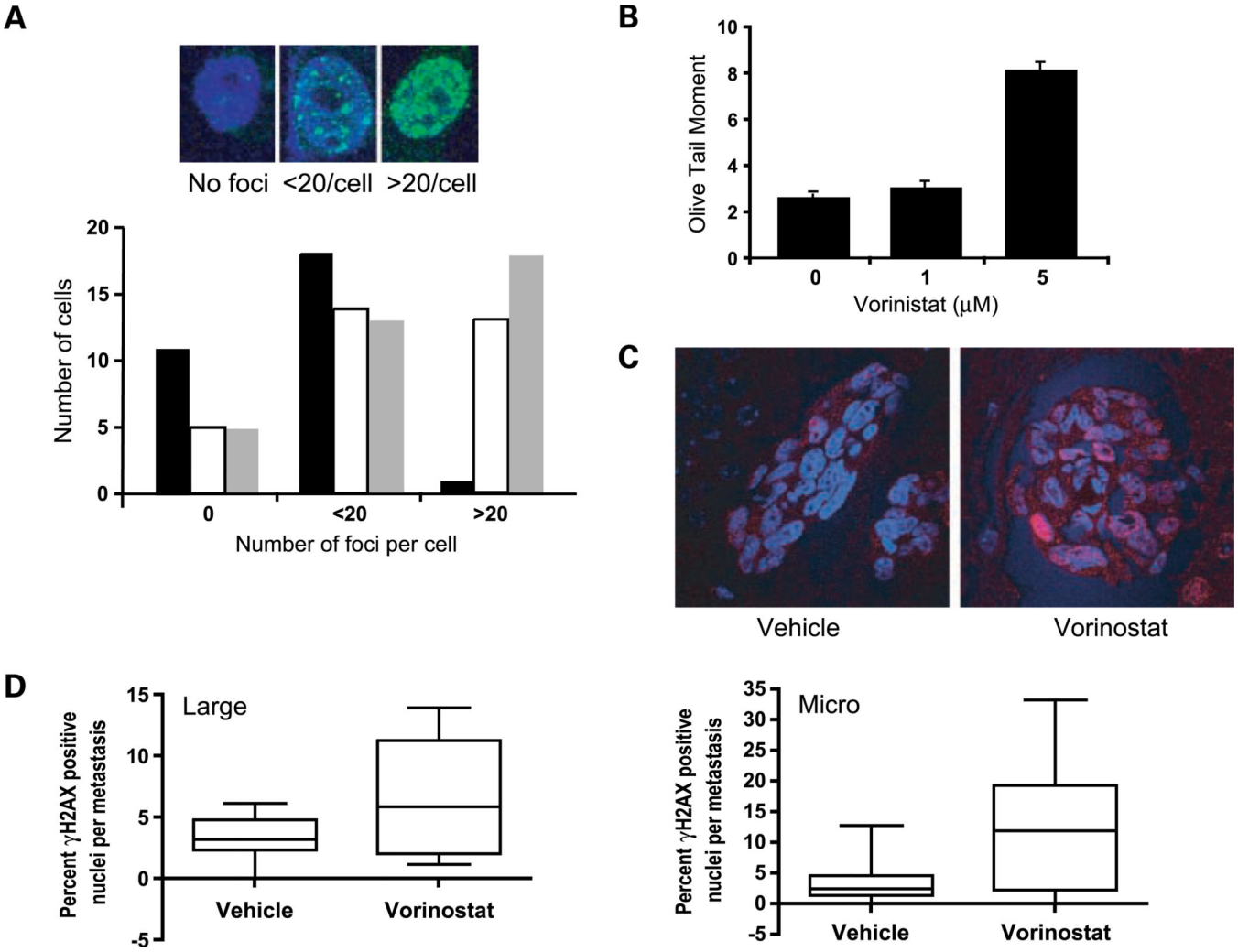

Fig. 4.

Vorinostat induces DNA damage *in vitro* and *in vivo*. *A*, *top*, representative immunofluorescent images of γ-H2AX foci (*green*) in the nucleus of vorinostat-treated 231-BR cells. Cells were treated with 1 μmol/L vorinostat or vehicle for 2 h. γ-H2AX immunofluorescence was done immediately following treatment or 24 h post-treatment. Nuclei were counterstained with 4′,6-diamidino-2-phenylindole. Magnification, ×400. *Bottom*, quantification of cells from γ-H2AX immunofluorescence. Cells were scored as having no foci, <20 foci per nucleus, or >20 foci per nucleus. *Black columns*, vehicle; *white columns*, 1 μmol/L vorinostat for 2 h; *gray columns*, 24 h after removal of 1 μmol/L vorinostat for 2 h. *B*, *in vitro* analysis of DNA DSB using the comet assay. 231-BR cells were treated with vehicle or 1 or 5 μmol/L vorinostat for 24 h. Mean olive tail moment pooled over three experiments. $P < 0.0001$ (vorinostat effect by ANOVA), post-hoc Dunnett's multiple comparison; $P = 0.34$ and $P < 0.0001$ for vehicle versus 1 and 5 μmol/L, respectively. *C*, representative images of immunofluorescent γ-H2AX staining in metastatic lesions. Frozen-fixed sections of mouse brains from vehicle- or vorinostat-treated mice were stained for γ-H2AX. Positive foci are visible in pink, and all nuclei were stained with 4′,6-diamidino-2-phenylindole. Magnification, ×400. *D*, *left*, quantification of γ-H2AX staining

in large metastases. The percentage of positively stained cells per large metastasis was calculated for all large metastases present in one section per mouse. Four or five mice were analyzed per group containing two to four large metastases per section. $P = 0.047$, weighted ANOVA. *Right*, quantification of γ-H2AX staining in micrometastases. The percentage of positively stained cells per micrometastasis was calculated. One section per mouse from five mice was analyzed per group with four to six micrometastasis per mouse. $P = 0.004$, weighted ANOVA.

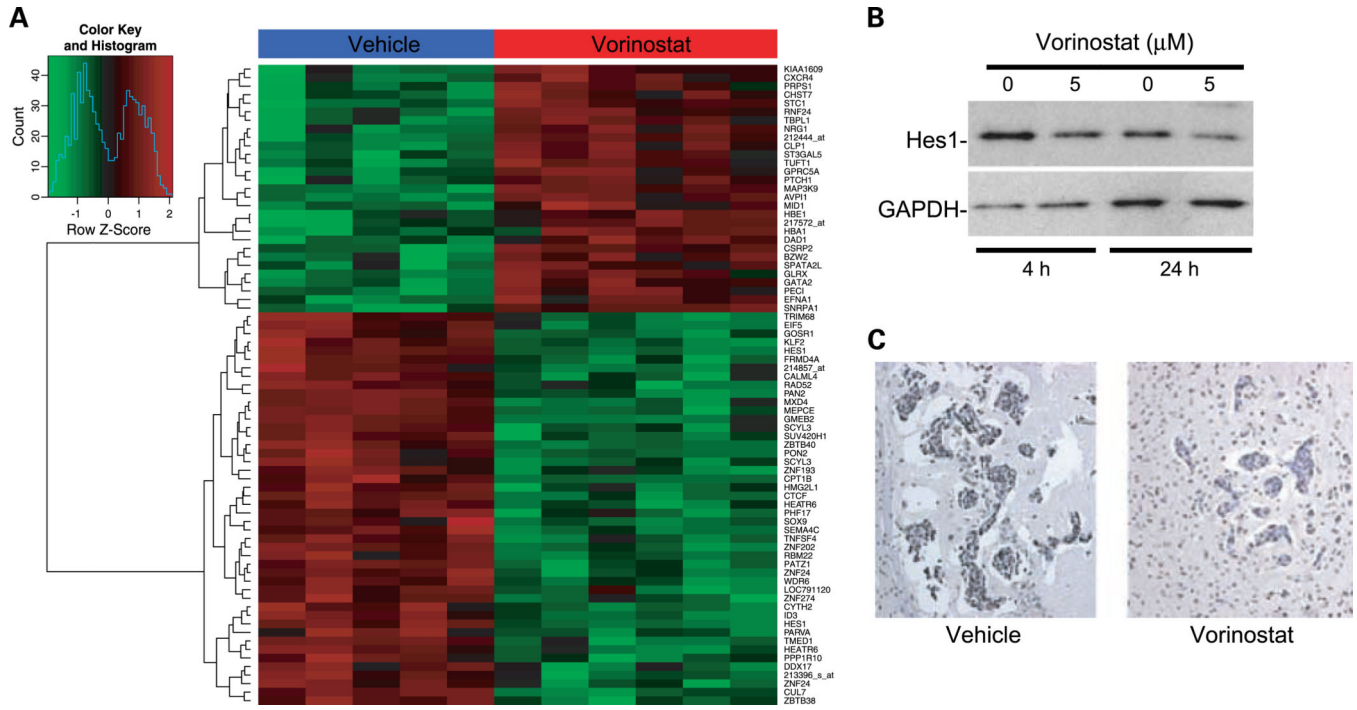

Fig. 5.

Analysis of gene expression changes induced by vorinostat treatment. *A*, a simple hierarchical clustering of the top 75 genes differentially expressed in the tumor cells of vorinostat-treated mice compared with vehicle controls. Tumor cells were laser capture microdissected from frozen tissue sections. RNA was extracted, amplified, labeled, and applied to Affymetrix Human U133A 2.0 GeneChips. Vorinostat-treated samples are labeled in red and vehicle samples are labeled in blue. *B*, Western blot validation of decreased Hes1 protein in response to vorinostat treatment. 231-BR cells were treated with 5 μmol/L vorinostat or vehicle for the times indicated. *C*, immunohistochemical validation of decreased Rad52 protein *in vivo*. Representative clusters of metastases from vorinostat- and vehicle-treated mice. Magnification, ×200. One section from each of five mice per group was analyzed.

Table 1.

Effect of treatment start day on the efficacy of vorinostat

Treatment start	*n*	Micrometastases		Large metastases*	
		Mean† (95% confidence interval)	*P*‡	Mean (95% confidence interval)	*P*
Vehicle	20	170 (146–193)		7.65 (6.20–9.10)	
Day 3 post-injection	18	122 (98–146)	0.017	2.89 (1.94–3.84)	<0.0001
Day 7 post-injection	19	151 (127–176)	NS	4.94 (3.90–5.98)	0.008
Day 14 post-injection	18	177 (153–201)	NS	5.96 (4.69–7.22)	NS

NOTE: 175,000 231-BR cells were injected into the left ventricle of the heart of BALB/c nude mice. Results of two experiments are combined.

Abbreviation: Not significant.

*Size of metastases was determined by a 16 mm^2 ocular grid. Large metastases are >300 μm on the longest axis.

†Mean number of metastases per section counted in 10-step sections from one hemisphere of the brain.

‡A two-factor factorial ANOVA was used to determine significance. All P values are two-tailed and adjusted for multiple comparisons using Dunnett's method.